

# Ceramic Waveguides

C. Yeh,<sup>1</sup> F. Shimabukuro,<sup>2</sup> P. Stanton,<sup>1</sup> V. Jamnejad,<sup>1</sup> W. Imbriale,<sup>1</sup> and F. Manshadi<sup>1</sup>

*This article is an expanded version of an original article published in Nature (April 6, 2000) entitled, "Millimeter/Submillimeter Wave Communications via Ceramic Ribbon." Finding a very low-loss waveguide in the millimeter-/submillimeter-wave range has been a problem of considerable interest for many years. Researching the fundamentals, we have found a new way to design a waveguide structure that is capable of providing an attenuation coefficient of less than 10 dB/km for the guided dominant mode. This structure is a ceramic (Coors' 998 alumina) ribbon with an aspect ratio of 10:1. This attenuation figure is more than one hundred times smaller than that for a typical ceramic or other dielectric circular-rod waveguide. It appears that the dominant transverse magnetic (TM)-like mode is capable of "gliding" along the surface of the ribbon with exceedingly low attenuation and with a power pattern having a dip in the core of the ribbon guide. This feature makes the ceramic ribbon a true "surface" waveguide structure wherein the wave is guided along, adhering to a large surface with only a small fraction of the power being carried within the core region of the structure. Here, through theoretical analysis as well as experimental measurements, the existence of this low-loss ceramic ribbon structure is proven. Practical considerations, such as an efficient launcher as well as supports for a long open ribbon structure, also have been tested experimentally.*

*The availability of such a low-loss waveguide may now pave the way for new development in this millimeter-/submillimeter-wave range.*

## I. Introduction

This article is an expanded version of an original article published in *Nature* (April 6, 2000) entitled, "Millimeter/Submillimeter Wave Communications via Ceramic Ribbon." Ever since the discovery by Kao and Hockman [1] that ultra-low-loss optical fiber can be made from pure silica through the elimination of impurities, the ability to guide signals in the optical spectrum with very low attenuation loss has been assured. There remains a spectrum from 30 GHz to 1000 GHz (called the millimeter-/submillimeter-wave band), where low-loss waveguides are still unknown. Because of the presence of inherent vibrational absorption bands in solids [2-4], the elimination of impurities is no longer the solution for finding low-loss

---

<sup>1</sup> Telecommunications Science and Engineering Division.

<sup>2</sup> The Aerospace Corporation, El Segundo, California.

The research described in this publication was carried out by the Jet Propulsion Laboratory, California Institute of Technology, under a contract with the National Aeronautics and Space Administration.

solids in this spectrum. High skin-depth loss [5,6] in this spectrum also eliminates the use of highly conducting material. It thus appears that it might be a futile effort to search for ultra-low-loss solids as ultra-low-loss waveguide material in this millimeter-/submillimeter-wave band.

The purpose of this article is to show a new way to obtain an ultra-low-loss waveguide structure for this millimeter-/submillimeter-spectrum band, to show the theoretical foundation for this discovery and experimental verification, to show why such a structure is a low-loss structure, and to display its low-loss and power-guiding characteristics.

## II. Theoretical Foundation

According to the theory of wave propagation along a dielectric waveguide, the attenuation constant,  $\alpha$ , of a dielectric waveguide surrounded by dry air is given by the following formula [7,8]:

$$\alpha = 8.686\pi \left( \frac{1}{\lambda_0} \right) (\varepsilon_1 R \tan \delta_1) \quad (1)$$

in dB/m, where

$$R = \frac{\int_{A_1} (\mathbf{E}_1 \times \mathbf{E}_1^*) dA}{\left( \frac{\mu}{\varepsilon_0} \right)^{1/2} \left[ \int_{A_1} \mathbf{e}_z \times (\mathbf{E}_1 \times \mathbf{H}_1^*) dA + \int_{A_0} \mathbf{e}_z \times (\mathbf{E}_0 \times \mathbf{H}_0^*) dA \right]} \quad (2)$$

Here,  $\varepsilon_1$  and  $\tan \delta_1$  are, respectively, the relative dielectric constant and the loss tangent of the dielectric core material;  $\mu$  and  $\varepsilon_0$  are, respectively, the permeability and permittivity of free-space;  $\lambda_0$  is the free-space wavelength in meters;  $\mathbf{e}_z$  is the unit vector in the direction of propagation;  $A_1$  and  $A_0$  are, respectively, the cross-sectional areas of the core and the cladding region; and  $(\mathbf{E}_1, \mathbf{H}_1)$  and  $(\mathbf{E}_0, \mathbf{H}_0)$  are, respectively, the modal electric and magnetic field vectors of the guided mode in the core region and in the cladding region. One notes that the factor  $\varepsilon_1 R$  is defined as the geometrical loss factor and the attenuation factor,  $\alpha$ , is directly proportional to it.

### A. Normal-Mode Solution

The normal-mode fields for a given guiding structure are the eigenfields, which are obtained from the eigenvalues and eigensolutions of the wave equation corresponding to the appropriate boundary conditions [5,6]. The exact analytic solutions for a dielectric waveguiding structure are known only for a planar dielectric slab, for a circular dielectric cylinder (such as a typical optical fiber), and for an elliptical dielectric cylinder [7,8]. Numerical techniques, such as the finite-element technique [9], the finite difference time domain technique [10], or the beam-propagation technique [11], must be used for other geometrical shapes. Only hybrid modes with all six field components can be supported by non-circular dielectric waveguides [7,8].

To find the normal-mode solution for arbitrarily shaped dielectric waveguides, an exact approach based on the solution of Maxwell's equations by the finite-element method is used. This method has been used successfully to analyze single-mode optical waveguides [9–11]. According to this finite-element approach [9–11], the governing longitudinal fields of the guided wave are first expressed as a functional as follows:

$$\begin{aligned}
I &= \sum_p I_p \\
&= \sum_p \iint \left\{ \tau_p \left| \nabla H_z^{(p)} \right|^2 + \gamma^2 \tau_p \varepsilon_p \left| \frac{(\mu/\varepsilon_0)^{-1/2}}{\gamma} \nabla E_z^{(p)} \right|^2 + 2\gamma^2 \tau_p \mathbf{e}_z \times \left| \frac{(\mu/\varepsilon_0)^{-1/2}}{\gamma} \nabla E_z^{(p)} \times \nabla H_z^{(p)} \right| \right. \\
&\quad \left. - \left( \frac{\omega}{c} \right)^2 (\gamma^2 - 1) \left[ \left( H_z^{(p)} \right)^2 + \gamma^2 \frac{\varepsilon_p}{\varepsilon_0} \left[ \frac{(\mu/\varepsilon_0)^{-1/2}}{\gamma} E_z^{(p)} \right]^2 \right] \right\} dx dy \tag{3}
\end{aligned}$$

where

$$\begin{aligned}
\gamma &= \frac{\beta c}{\omega} \\
\tau_p &= \frac{(\gamma^2 - 1)}{(\gamma^2 - \varepsilon_p)}
\end{aligned}$$

Here  $\varepsilon_p$  is the relative dielectric constant in the  $p$ th region;  $\beta$  is the propagation constant;  $\omega$  is the frequency of the wave;  $\mathbf{e}_z$  is a unit vector in the  $z$  direction;  $(x, y)$  are the cross-sectional coordinates; and  $c$  is the speed of light in a vacuum. The symbol  $p$  represents the  $p$ th region when one divides the guiding structure into appropriate regions. Minimizing the above surface integral over the whole region is equivalent to satisfying the wave equation and the boundary conditions for  $E_z$  and  $H_z$ . In the finite-element approximation, the primary dependent variables are replaced by a system of discrete variables over the domain of consideration. There, the initial step is to divide the original domain into many discrete subregions. For the present analysis, there are a number of regions in the composite cross section of the ribbon waveguide for which the permittivity (dielectric constant) is distinct. Each of these regions is made into a number of discrete smaller triangular subregions interconnected at a finite number of points, called nodes. Appropriate relationships then can be developed to represent the waveguide characteristics in all triangular subregions. These relationships are assembled into a system of algebraic equations governing the entire cross section. Taking the variation of these equations with respect to the nodal variable leads to an algebraic eigenvalue problem from which the propagation constant for a certain mode may be determined. The longitudinal electric field,  $E_z^{(p)}$ , and the longitudinal magnetic field,  $H_z^{(p)}$ , in each subdivided  $p$ th region also are generated in this formalism. All transverse fields in the  $p$ th region subsequently can be produced from the longitudinal fields. A complete knowledge of the fields can be used to generate the geometrical loss factor according to Eq. (2). This is the method [9–11] we used to generate all our theoretical results.

## B. Geometrical Loss Factor

Examination of the fundamental equation [Eq. (1)] governing the attenuation constant of a dominant mode guided by a simple solid dielectric waveguide surrounded by lossless dry air shows that it is dependent on the loss factor and the dielectric constant of the dielectric material and the geometrical size and shape of the guiding structure [7,8,12]. (See Fig. 1). Since the material loss factor and the dielectric constant of a solid are fixed, the only way to reduce the attenuation constant is to find the proper cross-sectional geometry of the waveguide. After performing a systematic study on a variety of geometries, our research shows that a ribbon-shaped guide made with low-loss, high-dielectric-constant ceramic material, such as alumina, can yield an attenuation constant for the dominant transverse magnetic (TM)-like mode of less than 0.005 dB/m. (Two dominant modes with no cutoff frequency can be supported by this ceramic ribbon structure [7,8]: a transverse electric (TE)-like dominant mode with most of its electric

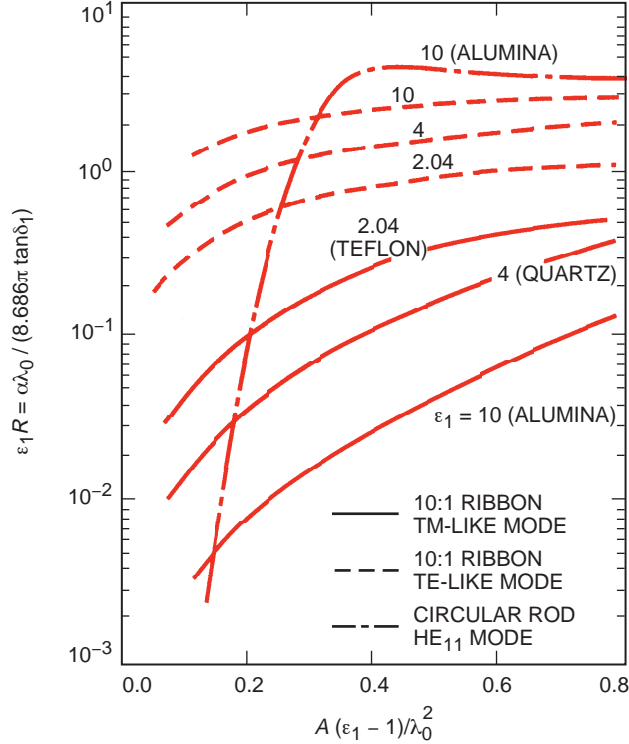


**Fig. 1. The geometrical loss factor  $\epsilon_1 R$  as a function of the normalized cross-sectional area  $A(\epsilon_1 - 1)/\lambda_0^2$ .**

field aligned parallel to the major axis of the ribbon and a TM-like dominant mode with most of its electric field aligned parallel to the minor axis of the ribbon.) As a comparison, at an operating frequency band around 100 GHz, one finds the attenuation constant for the traditional Teflon dielectric waveguide at 1.3 dB/m, for the usual metallic rectangular waveguide at 2.4 dB/m, and for the microstripline at 3 dB/m [13]. This remarkable low-loss behavior of a ceramic ribbon guiding the dominant TM-like mode is shown in Fig. 1, where  $A$  is the cross-sectional area of the waveguide,  $\epsilon_1$  is the relative dielectric constant of the dielectric guide, and  $\lambda_0$  is the free-space wavelength. Dielectric ribbons with aspect ratios of 10 and an alumina circular rod are considered. For the ribbon case, the geometrical loss factors for the dominant TM-like (low-loss) and TE-like (high-loss) modes are obtained for three different dielectric materials: alumina with  $\epsilon_1 = 10$ , quartz with  $\epsilon_1 = 4$ , and Teflon with  $\epsilon_1 = 2.04$ . The case for the alumina circular rod is displayed for comparison purposes. It is seen that alumina ribbon supporting the TM-like mode provides the most dramatic reduction in the geometrical loss factor as compared with that for the alumina circular rod. Suitable choice of configuration and dielectric constant can significantly reduce the geometrical loss factor for the TM-like mode. Several important conclusions can be drawn from the results given in Fig. 1:

- (1) Dramatically lower geometrical loss factors are obtained for a high-aspect-ratio ribbon waveguide with a high dielectric constant. As an example, when the normalized cross-sectional area,  $A(\epsilon_1 - 1)/\lambda_0^2$ , is 0.4, the geometrical loss factor (as well as the attenuation factor) for this ribbon supporting the dominant TM-like mode is about 140 times smaller than that for a circular rod with the same cross-sectional area supporting the dominant  $HE_{11}$  mode.
- (2) To achieve this dramatically lower geometrical loss factor, the guiding structure must be of ribbon shape with a high aspect ratio as well as a high dielectric constant, supporting the dominant TM-like mode.

- (3) In the low-loss region, i.e.,  $\varepsilon_1 R < 0.05$ , the geometrical loss factor curve for the 10:1 ribbon with dielectric constant  $\varepsilon_1 = 10$  supporting the TM-like mode is much flatter than that for the circular rod supporting the  $\text{HE}_{11}$  mode, indicating that the geometrical loss factor for the ribbon is insensitive to small deviations of the normalized cross-sectional area of the ribbon while the geometrical loss factor for the circular rod is very sensitive to size changes in the rod. This means the TM-like mode on the ribbon is a very stable mode, not easily disturbed by any geometrical imperfections.
- (4) Separation of the geometrical loss curves for the TE-like mode and the TM-like mode becomes larger for a larger dielectric constant of the guiding ribbon. And, there is a definite relationship between the geometrical loss curves for the TE-like mode and that for the TM-like mode. These facts are very significant, because they can be used to devise a fundamentally new way to measure the super-low-loss characteristics of the TM-like mode guided along ceramic ribbon.
- (5) Inspection of the expression for the geometrical loss factor, Eq. (2), shows that the numerator term representing the electric field intensity within the dielectric waveguide governs the magnitude of the geometrical loss factor. To minimize this factor, the electric field intensity must be chosen to be as small as possible over the cross-sectional area of the dielectric guide. It is noted that the TM-like mode on a ribbon structure provides precisely this behavior while the opposite is true for the TE-like mode on this structure. Thus, the TE-like mode yields a much higher geometrical loss factor than does the TM-like mode.

### C. Relationship Between Geometrical Loss Factors for the TE-Like Mode and the TM-Like Mode

Let us now investigate the relationship between the geometrical loss factors for the TE-like mode and for the TM-like mode on a high-aspect-ratio ribbon. The ratio  $r_\alpha$  is introduced and defined as follows:

$$r_\alpha = \frac{(\varepsilon_1 R)_{\text{TE-like}}}{(\varepsilon_1 R)_{\text{TM-like}}} \quad (4)$$

$$= \frac{\alpha_{\text{TE-like}}}{\alpha_{\text{TM-like}}} \quad (5)$$

This ratio is displayed in Fig. 2, where  $A$  is the cross-sectional area of the waveguide,  $\varepsilon_1$  is the relative dielectric constant of the dielectric guide, and  $\lambda_0$  is the free-space wavelength. It is seen that for high-dielectric-constant ribbon material, such as  $\varepsilon_1 = 10$ , the ratio may be quite high, implying that the attenuation for the dominant TM-like mode and that for the dominant TE-like mode can be different by two orders of magnitude. For example, when the normalized area  $A(\varepsilon_1 - 1)/\lambda_0^2$  is 0.4,  $r_\alpha$  is about 88, implying that the attenuation constant for the TM-like mode can be 88 times smaller than that for the TE-like mode on the same ribbon structure. This relationship will be used (later) to measure the very low attenuation factor for the TM-like mode on a ribbon.

### D. External Field Decay Consideration

Having established theoretically the fact that the geometrical factor  $\varepsilon_1 R$  can be significantly reduced with the choice of high-dielectric-constant core material for the waveguide as well as the choice of a thin ribbon geometry, it is important to answer the question of whether even higher dielectric-constant material can provide an even smaller (or better)  $\varepsilon_1 R$  factor. In order to answer this question, it is important to mention that, for an open waveguide structure such as the dielectric waveguide, the field extent (or field decaying rate) away from the guiding structure represents a very important measure of how well the structure “guides” the wave. So, one must rephrase the question: For a given (same) field decaying rate

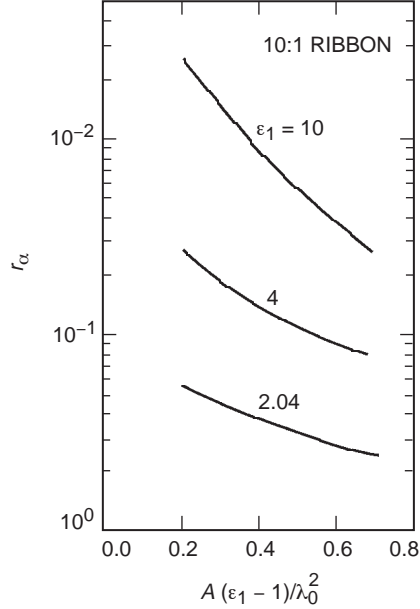


**Fig. 2. The ratio  $r_\alpha$  as a function of the normalized cross-sectional area  $A(\epsilon_1 - 1)/\lambda_0^2$  for a 10:1 ribbon waveguide for three different ribbon materials with  $\epsilon_1 = 10, 4,$  and  $2.04$ .**

away from the surface of the dielectric core, will a higher-dielectric-constant material yield a smaller  $\epsilon_1 R$ ? Figure 3 is developed to address this question. In this figure,  $\epsilon_1 R$  is plotted as a function of the dielectric constant of the core for a fixed decaying rate of unity normalized to the free-space wavelength for the exterior field from the core surface. (This decaying rate means that the exterior field would have been reduced by  $1/e$  at one free-space wavelength from the guiding surface. Our experiment shows that the guided field is still very well bonded to the guiding structure at this decaying rate.) It is seen that  $\epsilon_1 R$  initially reduces very rapidly as the dielectric constant is increased, reaching a minimum between 10 and 14. Then,  $\epsilon_1 R$  increases very gently for further increase in the dielectric constant. Hence, core material with a dielectric constant of around 10 appears to be the preferred choice. For a smaller normalized decaying rate (i.e., for weaker guidance), the curve in Fig. 3 moves lower and shifts slightly towards a higher dielectric constant. This implies that  $\epsilon_1 R$  can be made even smaller, but at the expense of much weaker guidance. In that case, somewhat higher dielectric-constant material should be used to obtain the lowest value of  $\epsilon_1 R$ . Keeping the normalized decaying rate higher than unity, the choice of alumina with a dielectric constant of 10 appears to be the optimum.

Having established theoretically that there exists a low-loss geometry for a dielectric waveguide, we must verify this discovery experimentally.

### III. Experimental Verification

It is known that the cavity resonator method provides a very sensitive and accurate way of measuring the attenuation of very low-loss waveguides [14]. For the present case, the resonator used for the experimental measurements consists of a dielectric waveguide placed in a parallel metallic plate cavity. A swept signal frequency is transmitted through the waveguide cavity and is detected by a network analyzer. The signals are coupled through very small (below cutoff) holes in the circular gold-plated reflectors.

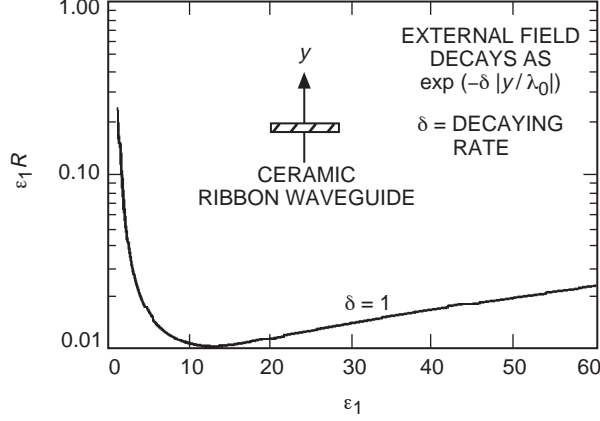


**Fig. 3.** The geometrical loss factor,  $\epsilon_1 R$ , as a function of the dielectric constant,  $\epsilon_1$ , of the 10:1 ribbon waveguide for a fixed decaying rate of unity normalized to the free-space wavelength for the exterior field from the core surface of the guide.

The plates (15.24 cm in diameter) are much larger than the field extent outside the dielectric waveguide. A picture of this resonator is provided in Fig. 4. The output is a series of narrow transmission resonances at  $f_1, f_2, \dots, f_m$  with half-power bandwidths  $\Delta f_1, \Delta f_2, \dots, \Delta f_m$ , respectively. Here, the symbol  $f$  represents frequency. At each resonant frequency, the guide wavelength is given by

$$\lambda_{gm} = \frac{2L}{m} \quad (6)$$

and  $Q$  is given by

$$Q_m = \frac{f_m}{\Delta f_m} \quad (7)$$

where  $m$  is an integer number representing the  $m$ th resonance, and the integer  $m$  also represents the number of guide half-wavelengths at a particular resonant frequency.

With careful alignment of the dielectric ribbon waveguide and the shorting plates, the primary loss mechanisms to be considered are the wall losses and the dielectric loss. It is known [14] that

$$\frac{1}{Q_m} = \frac{1}{Q_d} + \frac{1}{Q_w} \quad (8)$$

Here,  $Q_m$  is the measured  $Q$  of the  $m$ th mode;  $Q_d$  is the contribution of cavity  $Q$  due to dielectric waveguide loss, which is independent of the length,  $L$ , of the cavity; and  $Q_w$  is the contribution of cavity  $Q$  due to the metal-wall losses of the shorting plates and the coupling losses. These losses are linearly proportional to the length  $L$  of the cavity. For the various dielectric waveguides of interest, the calculated  $Q_w$  ranges from 10,000  $L$  to 20,000  $L$ , where  $L$  is the cavity length in centimeters. Experimentally, the effect of the wall losses, whether due to the coupling or to the ohmic dissipation, on the cavity  $Q$  could not be detected provided that  $Q_d < 30,000$ , i.e.,

$$Q_w \gg Q_d \quad (9)$$

Under this condition,  $Q = Q_d$ .



Fig. 4. The alumina ribbon waveguide resonator with small, below-cutoff coupling holes in the gold-plated parallel plates at the ends of the white alumina ribbon. This setup is used to measure the  $Q$  for the TE-like or TM-like mode supported by the alumina ribbon. In the background is the HP 8510 measuring instrument with the display of a resonant curve.

### A. Relation Between $\alpha$ and $Q$

The relation between  $\alpha$  and  $Q$  has been derived earlier [15]:

$$\alpha = 8.686 \left( \frac{v_p}{v_g} \right) \left( \frac{\beta}{2Q} \right) \quad (10)$$

$$= \left( \frac{8.686\pi}{Q} \right) \left( \frac{v_g}{c} \right) \left( \frac{1}{\lambda_0} \right) \quad (11)$$

in dB/m, where  $\beta$  is the propagation constant of the mode under consideration;  $v_p$  is the phase velocity of that mode;  $v_g$  is the group velocity of that mode;  $c$  is the speed of light in a vacuum; and  $\lambda_0$  is the free-space wavelength. For the hybrid HE(even) (TM-like) or HE(odd) (TE-like) mode on a dielectric waveguide such as the dielectric ribbon, explicit analytic relations for  $\beta$ ,  $v_p$ , and  $v_g$  do not exist [7,8]. They may, however, be obtained numerically for that mode. It can be shown [14] that, for the dominant hybrid mode, at low frequencies or small  $\beta$ ,  $v_p \approx v_g$ , and, again, at very high frequencies or large  $\beta$ ,  $v_p \approx v_g$ . So, the relation  $\alpha = 8.686(\beta/2Q)$  is applicable to the dominant hybrid modes at very low frequencies or at very high frequencies. The more general expression, Eq. (10), must be used for all other frequencies.

### B. A New Way To Measure the $Q$ of the TM-Like Mode

The relationship between the attenuation constants for the TM-like mode and the TE-like mode on a dielectric ribbon has been found and is displayed in Fig. 2. Using Eq. (10), one finds

$$\begin{aligned}
r_\alpha &= \frac{(\varepsilon_1 R)_{\text{TE-like}}}{(\varepsilon_1 R)_{\text{TM-like}}} \\
&= \left( \frac{\alpha_{\text{TE-like}}}{\alpha_{\text{TM-like}}} \right) \\
&= \left( \frac{Q_{\text{TM-like}}}{Q_{\text{TE-like}}} \right) \left( \frac{v_{g\text{TM-like}}}{v_{g\text{TE-like}}} \right)
\end{aligned} \tag{12}$$

where  $v_{g\text{TE-like}}$  and  $v_{g\text{TM-like}}$  are, respectively, the group velocity of the TE-like mode and the TM-like mode, and  $Q_{\text{TE-like}}$  and  $Q_{\text{TM-like}}$  are, respectively, the  $Q$  for the TE-like mode and the TM-like mode.

A specific example will now be considered. Plots of  $(Q_{\text{TM-like}}/Q_{\text{TE-like}})$ ,  $(v_{g\text{TM-like}}/v_{g\text{TE-like}})$ ,  $(v_{g\text{TM-like}}/c)$ ,  $(v_{p\text{TM-like}}/c)$ ,  $(v_{g\text{TE-like}}/c)$ , and  $(v_{p\text{TE-like}}/c)$  versus frequency for a dielectric ribbon with an aspect ratio of 10 and cross-sectional dimensions of 0.0635 cm (thickness)  $\times$  0.635 cm (width) are shown in Fig. 5, where  $Q_{\text{TM-like}}$ ,  $v_{g\text{TM-like}}$ ,  $v_{p\text{TM-like}}$  and  $Q_{\text{TE-like}}$ ,  $v_{g\text{TE-like}}$ ,  $v_{p\text{TE-like}}$  are, respectively, the resonant  $Q$ , the group velocity, and the phase velocity of the TM-like and TE-like modes, and  $c$  is the velocity of light in a vacuum. It is seen that the ratio  $(Q_{\text{TM-like}}/Q_{\text{TE-like}})$  for an alumina ribbon can vary from a high of 42 at 30 GHz to 15 at 40 GHz. This means that, for a low-loss alumina ribbon with a loss tangent of 0.00005, if  $Q_{\text{TE-like}}$  is measured at 22,760 at 30 GHz (this  $Q$  value is well within the measurement capability of our apparatus),  $Q_{\text{TM-like}}$  must be 955,900 (this  $Q$  value is well beyond the measurement capability of any known room-temperature resonant cavity apparatus). A sample of Coors' alumina ribbon [16] with an aspect ratio of 10 and a cross-sectional area of 0.0635 cm  $\times$  0.635 cm and a sample of an alumina rod [16] with the same cross-sectional area are pictured in Fig. 6.

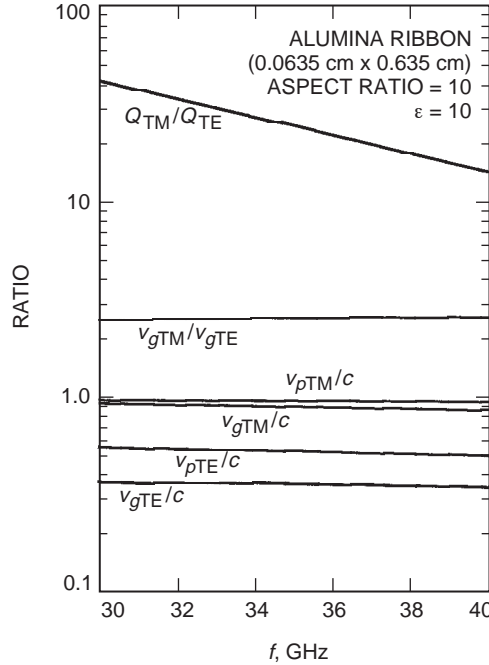


**Fig. 5. Ratios of  $Q_{\text{TM}}/Q_{\text{TE}}$ ,  $v_{g\text{TM}}/v_{g\text{TE}}$ ,  $v_{p\text{TM}}/c$ ,  $v_{g\text{TM}}/c$ ,  $v_{p\text{TE}}/c$ , and  $v_{g\text{TE}}/c$  versus the frequency  $f$ . Here the subscript TM or TE means TM-like or TE-like.**

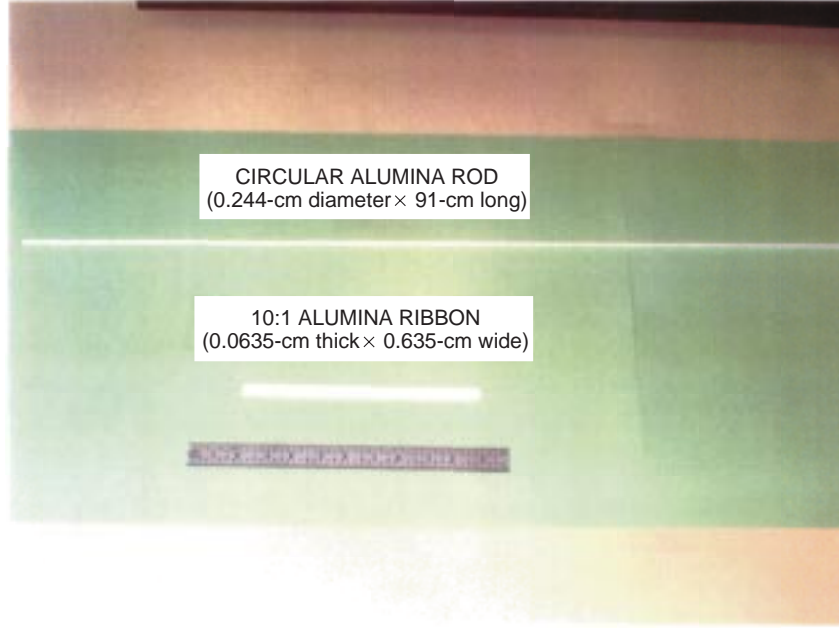


**Fig. 6. A section of alumina ribbon with an aspect ratio of 10 and a section of alumina circular rod with the same cross-sectional area.**

The fact that there is a definite relationship between  $Q_{\text{TM-like}}$  and  $Q_{\text{TE-like}}$  is quite important. This means that, knowing  $Q_{\text{TE-like}}$ , one may obtain  $Q_{\text{TM-like}}$ . Since  $Q_{\text{TE-like}}$  is normally much lower than  $Q_{\text{TM-like}}$  for a high-aspect-ratio and high-dielectric-constant ribbon, it is much easier and more accurate to measure  $Q_{\text{TE-like}}$ . This offers a new way to measure the very high values of  $Q_{\text{TM-like}}$  for a low-loss alumina ribbon, which, otherwise, may not be measurable due to the limitation placed by coupling and reflecting plate losses. It is, therefore, important to verify this relationship or the ratio ( $Q_{\text{TM-like}}/Q_{\text{TE-like}}$ ). For ease of measurement and to assure that the measured parameters are well within the capability of our apparatus, relatively higher loss ceramic ribbon samples are used. The sample is made by coating a  $0.0635\text{-cm} \times 0.635\text{-cm} \times 11.43\text{-cm}$  low-loss alumina ribbon with a thin layer of carbon particles. (See Fig. 7.) The thickness of the layer controls the loss tangent of the sample, which will govern how high the  $Q$  will be. The parameters  $Q_{\text{TM}}$  and  $Q_{\text{TE}}$  are measured separately, and the ratio ( $Q_{\text{TM-like}}/Q_{\text{TE-like}}$ ) is then obtained. As an example, the measured resonant curves for the TM-like mode and the TE-like mode are given in Fig. 8. From this figure, one obtains the following: At 38.8 GHz,  $Q_{\text{TM-like}}(\text{measured}) = 1943$  and  $Q_{\text{TE-like}}(\text{measured}) = 123$ . So, at 38.8 GHz, the ratio  $Q_{\text{TM-like}}/Q_{\text{TE-like}}(\text{measured}) = 15.79$  while  $Q_{\text{TM-like}}/Q_{\text{TE-like}}(\text{theory}) = 15.8$ . At 32.7 GHz,  $Q_{\text{TM-like}}(\text{measured}) = 5046$  and  $Q_{\text{TE-like}}(\text{measured}) = 170$ . So, at 32.7 GHz, the ratio  $Q_{\text{TM-like}}/Q_{\text{TE-like}}(\text{measured}) = 29.7$  while  $Q_{\text{TM-like}}/Q_{\text{TE-like}}(\text{theory}) = 31$ . These excellent agreements between measured values and theoretical values show the correctness of the derived theoretical ratio  $Q_{\text{TM-like}}/Q_{\text{TE-like}}$ . This relationship can be used reliably to obtain  $Q_{\text{TM-like}}$  when  $Q_{\text{TE-like}}$  is known or vice versa. As will be demonstrated in the following, this realization is very important in providing direct measurement on the attenuation constant for very low-loss alumina ribbon supporting the low-loss TM-like mode.

This technique will now be used to measure the  $Q$  and the attenuation constant for the TM-like mode on ultra-low-loss alumina ribbon. Three batches of alumina material samples were obtained from the Coors Ceramic Company [16]. Batch one, made from Coors' Superstrate 996 S20-71 (99.6 percent, Hirel, thin-film substrate), contains ribbons with dimensions of  $0.0635\text{ cm} \times 0.635\text{ cm} \times 11.43\text{ cm}$ . Batch two, made from a Coors' extruded 998 alumina (99.8 percent alumina) rectangular rod, contains ribbons with dimensions of  $0.0635\text{ cm} \times 0.635\text{ cm} \times 91.44\text{ cm}$ . Batch three is a Coors' extruded 998 alumina (99.8 percent alumina) circular rod with dimensions of  $0.244\text{ cm}$  (diameter)  $\times 91.44\text{ cm}$  (length).

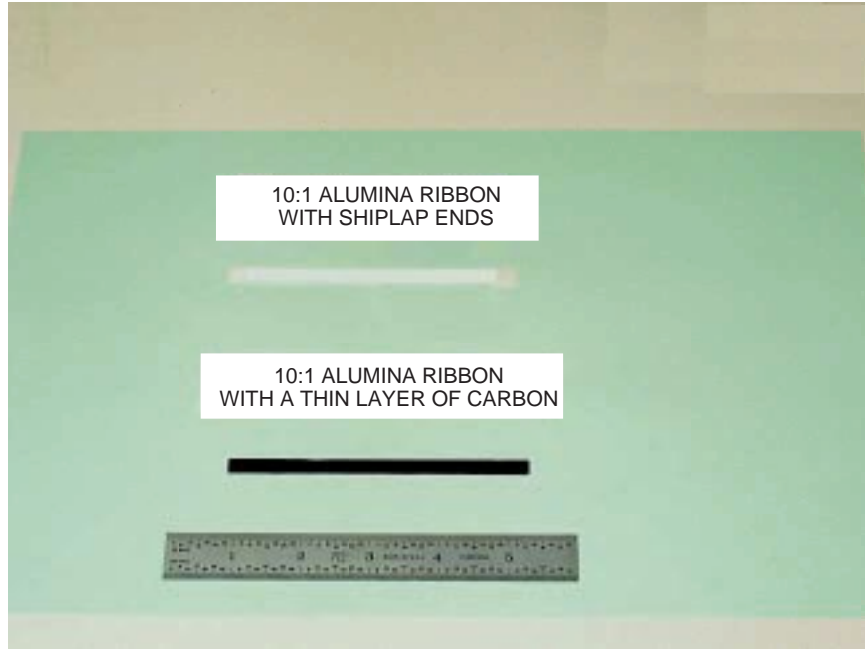


**Fig. 7.** A section of alumina ribbon coated with a thin layer of dried India ink (carbon powder) to induce higher loss and a section of alumina ribbon with shi lap ends to facilitate the connection between sections of alumina ribbon. The shi lap end is basically a 0.635-cm-long step, machined to a thickness of one-half the thickness of the ribbon.

Numerous repeated measurements were made on these samples at various frequencies within the frequency band from 30 to 40 GHz using the waveguide resonator technique described above. Typical results are given in Table 1. (See also Fig. 9.)

The uncertainty in the measured value is due to the uncertainty of the alignment with the coupling holes, the uncertainty in the flatness of the ribbon ends, and the uncertainty of the uniform thickness of the ribbon, etc. Since batch 3 contains a 91.44-cm-long circular alumina rod, the guiding property of the dominant mode is independent of the orientation of the transverse electric field. Thus,  $Q_{TE\text{-like}} = Q_{TM\text{-like}}$  for the circular rod. The importance of the geometrical factor is seen in the measured data. For example, the attenuation constant for an alumina ribbon with an aspect ratio of 10 is 0.0096 dB/m at 30 GHz while that for an alumina circular rod with the slightly larger cross-sectional area is 1.17 dB/m, which is 121 times larger, even though the alumina material for the circular rod is 30 percent less lossy than that for the ribbon. The measured results are displayed in Fig. 10, where excellent agreement between the experimental data and theoretical results can be seen. For dielectric waveguides made with alumina ( $\epsilon_1 = 10$ ) or Teflon ( $\epsilon_1 = 2.04$ ), the normalized cross-sectional area of these guides,  $A(\epsilon_1 - 1)/\lambda_0^2$ , is chosen to be 0.363, where  $A$  is the cross-sectional area,  $\epsilon_1$  is the dielectric constant of the guide, and  $\lambda_0$  is the free-space wavelength. The importance of the geometry of the guide is quite apparent from the curves. It can be seen from this figure that, at 30 GHz, the attenuation constant for this ribbon is 0.0098 dB/m, or less than 10 dB per kilometer, which is 165 times less than that for the dominant mode on an alumina circular rod with the same cross-sectional area. It is also 61 times less than that for the dominant mode in a standard metallic rectangular waveguide (WR 28). A two-fold improvement to less than 5 dB/km can easily be obtained for the ribbon if the same alumina material used for the circular rod were used.

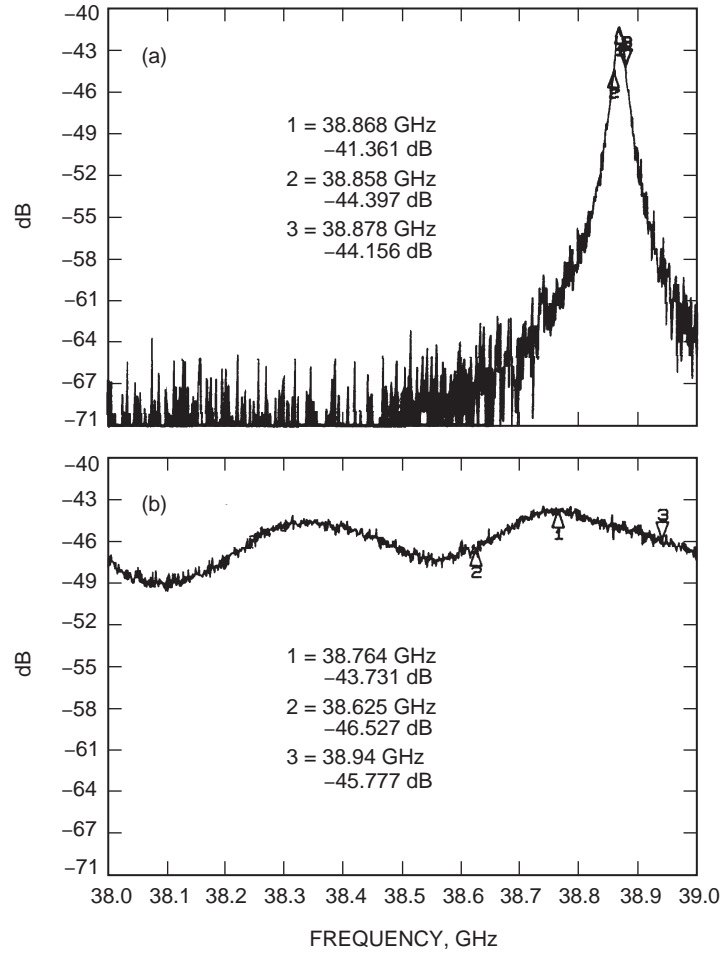


**Fig. 8. Resonant curves for a 10:1 aspect ratio, carbon-coated alumina ribbon with dimensions of 0.0635 cm x 0.635 cm x 11.43 cm supporting (a) a TM-like mode with  $Q_{TM} = 1943$  and (b) a TE-like mode with  $Q_{TE} = 123$ .**

**Table 1. Measured  $Q$  and  $\alpha$ .**

Batch number	Frequency, GHz	$Q_{TE-like}$	$Q_{TM-like}$	$\alpha_{TM}$ , dB/m	$\tan \delta$ ( $\times 10^{-4}$ )
1	38.60	$3,860 \pm 300$	$64,700 \pm 4,800$	$0.062 \pm 0.005$	$2.8 \pm 0.21$
1	32.80	$3,920 \pm 290$	$121,700 \pm 9,000$	$0.026 \pm 0.002$	$2.8 \pm 0.21$
2	38.89	$6,480 \pm 490$	$103,700 \pm 7,800$	$0.035 \pm 0.003$	$1.59 \pm 0.12$
2	32.98	$7,233 \pm 540$	$216,990 \pm 16,300$	$0.014 \pm 0.001$	$1.59 \pm 0.12$
3	39.96	$10,948 \pm 450$	$10,948 \pm 450$	$1.45 \pm 0.09$	$1.0 \pm 0.04$
3	30.03	$11,117 \pm 500$	$11,117 \pm 500$	$1.17 \pm 0.08$	$1.0 \pm 0.04$

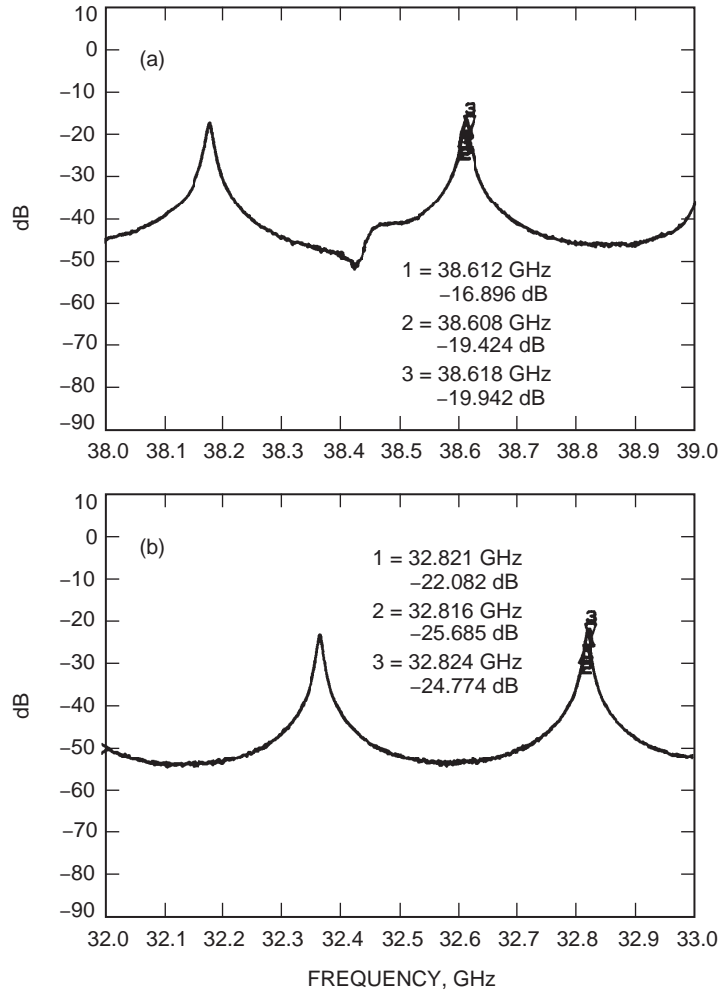


**Fig. 9. Resonant curves for a 10:1 aspect ratio, Coors ceramic Superstrate 996 alumina ribbon with dimensions of 0.0635 cm x 0.635 cm x 11.43 cm supporting (a) a TE-like mode with  $Q_{TE} = 3861$  at 38.612 GHz and (b) a TE-like mode with  $Q_{TE} = 3918$  at 32.821 GHz.**

## IV. Practical Considerations

### A. Experimental Evidence of Guidance by Ceramic Ribbon and Launching Efficiency

To show that guidance is indeed taking place along a ceramic ribbon, we have performed the following experiment: Shown in Fig. 11 are two horns, one transmitting and one receiving, separated by a free-space distance of 86 cm. A 120-ps pulse is emitted from the transmitting horn and is received by the receiving horn after traversing through this free-space distance of 86 cm. Another experiment is performed wherein a 91.44-cm-long ceramic ribbon waveguide is inserted between the horns. The horns are used to launch and receive the guided wave. Special transitions are used to maximize launching and receiving efficiencies. Launching (or receiving) efficiency of 84 percent (or a loss of less than 0.825 dB) at 39.86 GHz has been measured for an exponential launching horn. (See Fig. 12, where total transmission loss as low as 1.65 dB is obtained at 39.86 GHz. Most of this loss is due to launching (receiving) coupling loss. Propagation loss along the ribbon is less than 0.05 dB.) The same 120-ps pulse is sent through this ceramic ribbon waveguide structure. The received pulses for these two cases are displayed in Fig. 13, where the received pulse is displayed as pulse A. When the same pulse is sent through the same experimental setup without the

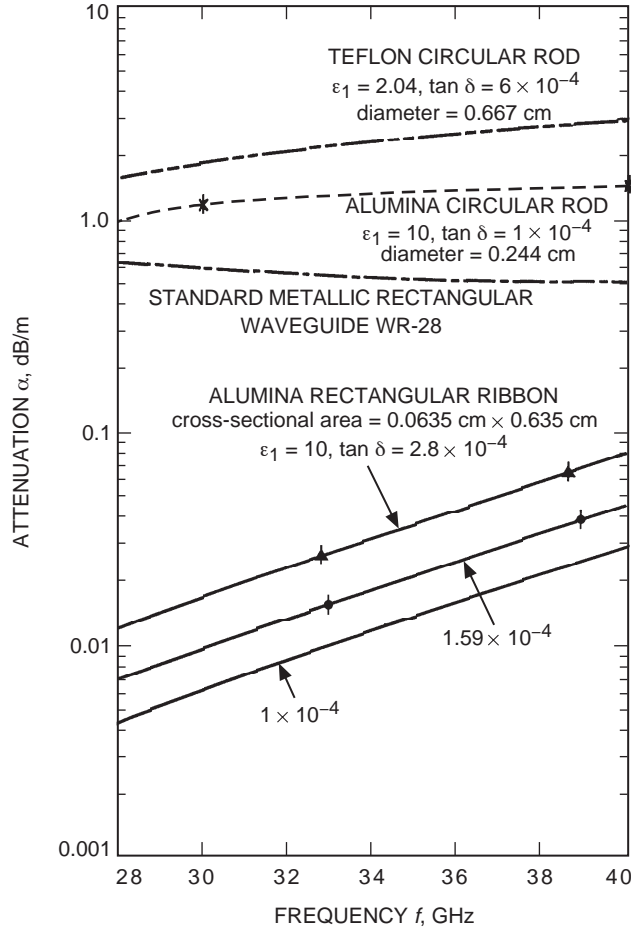


**Fig. 10. Attenuation constant  $\alpha$  for the low-loss dominant mode in various guiding structures versus frequency in the Ka-band. Experimentally measured values are displayed by data points while theoretical results are displayed by curves.**

alumina ribbon waveguide, the received pulse through free space is displayed as pulse B. The amplitude of pulse A is at least 21 dB larger than that of pulse B, proving that the alumina ribbon is indeed providing guidance for the pulse. The slight delay in the arrival of pulse A also indicates that, due to wave guidance by the alumina ribbon, pulse A is being guided by it and is propagating at the group velocity of the TM-like mode on this structure. This guided group velocity is slower than  $c$ , the free-space group velocity, as predicted and as shown in Fig. 5.

### B. Support for the Open Ceramic Ribbon Waveguide

The ceramic ribbon waveguide is an open structure surrounded by dry air. How to support such a structure is a problem of importance. One supporting structure appears to be most promising—support made with plastic fish lines. (See Fig. 14.) Thin plastic (low-dielectric-constant) fish lines, spaced 10 cm or longer apart, are strung across wooden rails separated by 5 cm (far enough apart so that the exterior guiding field at the ribbon edges has decayed to negligible value). Ceramic ribbon waveguide can simply be laid on top of the fish lines along the middle of the rails. The fish lines can amply support the ceramic ribbon. Any perturbation caused by the fish line support on the propagation characteristics of the guided TM-like mode on the ceramic ribbon waveguide is not detectable.

(a)



(b)

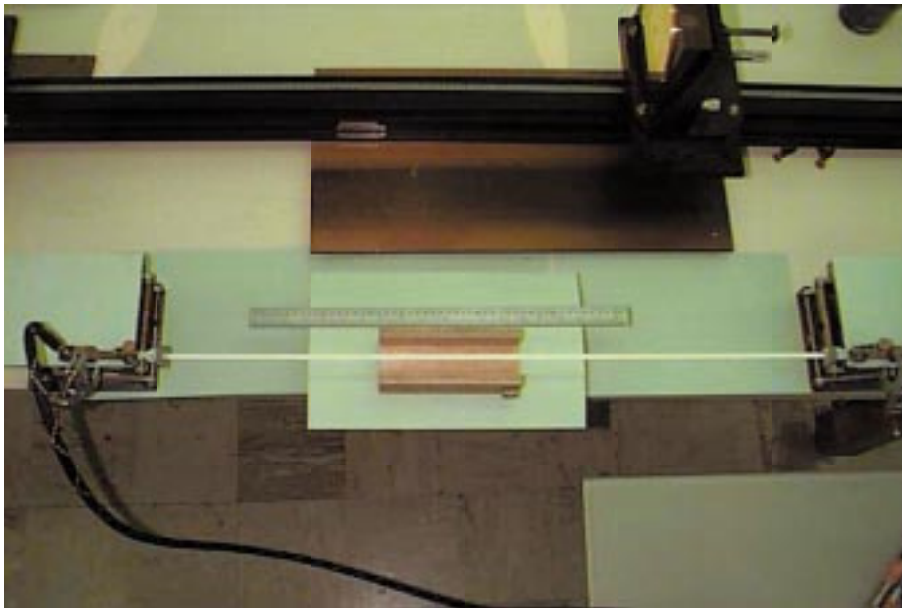


**Fig. 11.** Alumina ribbon waveguides with launching and receiving horns and cross-sectional areas of  $0.0635\text{ cm} \times 0.635\text{ cm}$ : (a) 40.64-cm long, shiplap connected with four pieces of 11.54-cm long alumina ribbon and (b) a 91.44-cm-long single piece. The structures are being supported by a fish-line supporting section (shown in the setups).

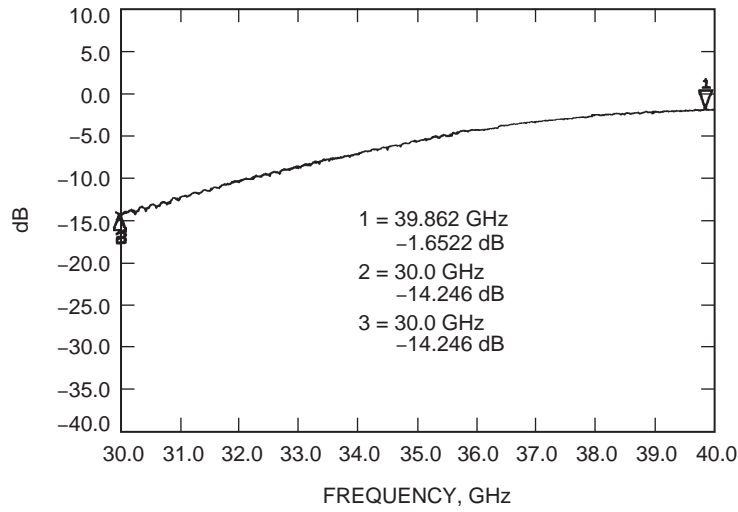


**Fig. 12.** Transmission coefficient  $S_{12}$  for the dominant TM-like mode as a function of frequency for the band from 30 to 40 GHz for the setup for an alumina ribbon waveguide as shown in Fig. 11(b).

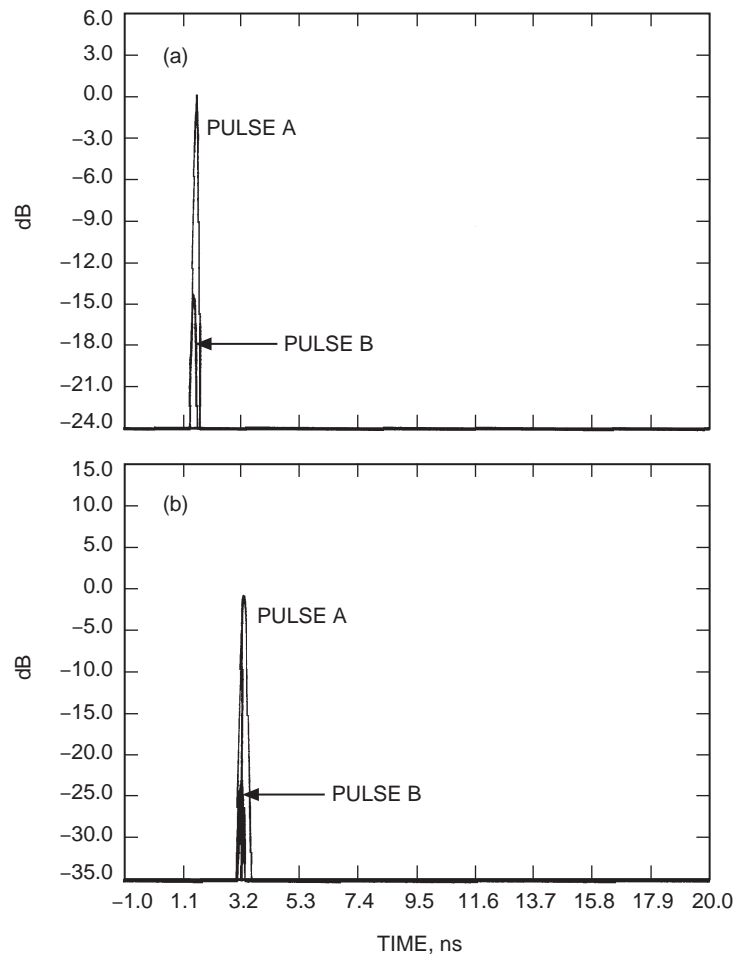


**Fig. 13.** A 120-ps pulse sent through the alumina ribbon waveguide setup shown in Fig. 11(a), supporting the TM-like dominant mode: (a) 40-cm long and (b) 91-cm long.



**Fig. 14. Details of the fish-line support. A separation of about 5.1 cm exists between the wooden rails, and a 3.81-cm clearance is present from the floor. These clearances are chosen so that the external surrounding field for the guided mode would not be affected by the wooden frame. Note also the almost seamless shiplap joints between sections of alumina ribbon.**

### C. Joining Sections of Ceramic Ribbon Waveguides

Another problem of practical importance is how to join sections of ceramic ribbon waveguides. We have discovered that a shiplap joint may be used to provide a strong connection between two ends of ceramic ribbon. A picture of the shiplap joint is shown in Fig. 7. A quarter-inch-long section of the jointing ribbon end is ground to a thickness of 0.032 cm, which is one-half the original thickness of the ribbon. The jointing end of the other ceramic ribbon is prepared similarly. The ends are lapped together, aligned, and then glued with “super glue,” resulting in a strong connection. No measurable loss due to the joint is found.

### V. Distribution of Guided Power and Discussion

To understand why the attenuation constant of the TM-like dominant mode is so much smaller than that of the TE-like dominant mode on the same ceramic ribbon structure, why it is so much smaller than that of the dominant HE mode on a circular ceramic waveguide [5,6] with the same cross-sectional area, and why the dielectric constant of the guiding structure plays such an important role in the low-loss guidance behavior, let us investigate the distribution characteristics of guided-power intensity for these two dominant modes on this ribbon structure.

To demonstrate the dramatic difference between the power-guiding characteristics of the TM-like and TE-like modes for a ceramic (high-dielectric-constant) ribbon waveguide and for a Teflon (low-dielectric-constant) ribbon waveguide, Fig. 15 is generated. In it, the power distribution characteristics of the two dominant modes (the TM-like mode and the TE-like mode) on a 10:1 aspect-ratio alumina ribbon with  $\epsilon_1 = 10$  and on a 10:1 aspect-ratio Teflon ribbon with  $\epsilon_1 = 2.04$  are shown. The cross-sectional sizes of these ribbons are chosen for single-mode operation at 40 GHz. The most distinguishing feature of Figs. 15(a) through 15(d) is that, for TM-like mode guidance, there is a dip in the power intensity in the thin alumina guiding ribbon. This distinctive feature is very much unlike the expected traditional feature for guided-power distribution along a circular dielectric waveguide where the guided-power intensity of the mode tends to peak in the middle of the guide and fall off as one moves away from the guide boundary.

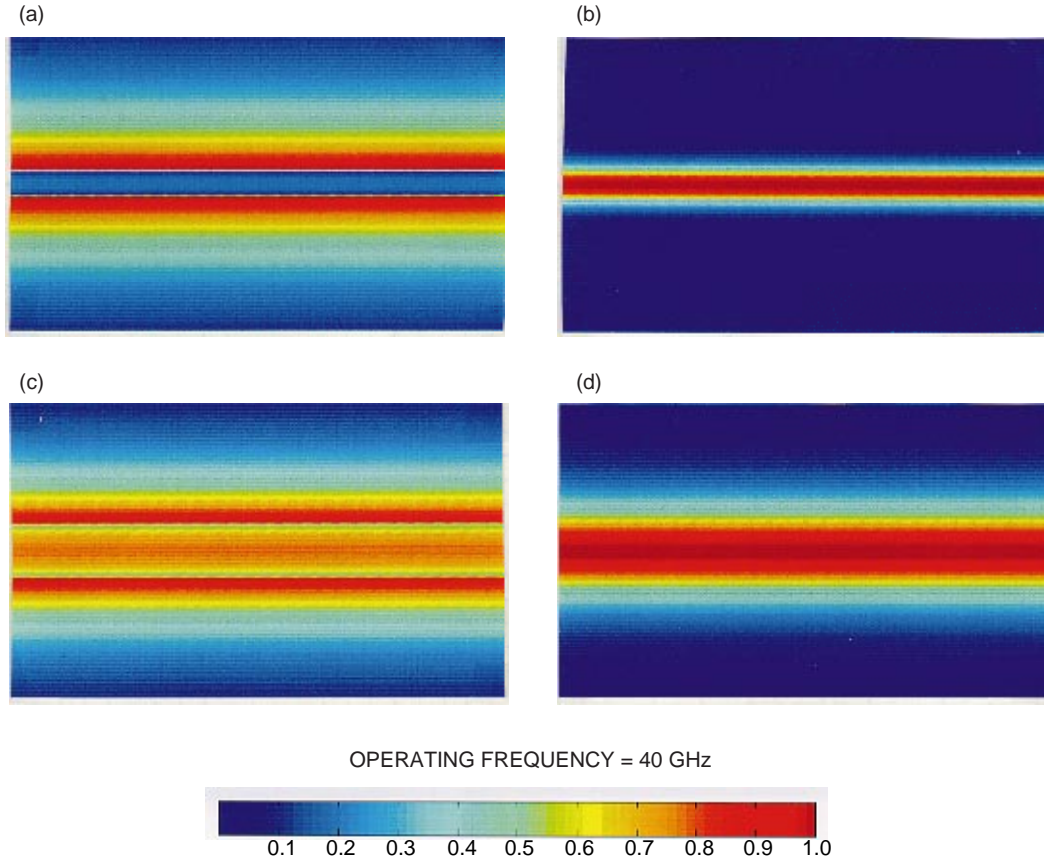


**Fig. 15. Normalized power-intensity distribution for the dominant normal modes on 10:1 dielectric ribbon structures. The highest power intensity is in red and the lowest in blue: (a) TM-like mode, alumina ribbon,  $\epsilon_1 = 10$ , ribbon thickness = 0.0625 cm, (b) TE-like mode, alumina ribbon,  $\epsilon_1 = 10$ , ribbon thickness = 0.0625 cm, (c) TM-like mode, Teflon ribbon,  $\epsilon_1 = 2.04$ , ribbon thickness = 0.317 cm, and (d) TE-like mode, Teflon ribbon,  $\epsilon_1 = 2.04$ , ribbon thickness = 0.317 cm.**

The traditional view is that this behavior remains regardless of how thin or small the guiding structure becomes or how large the dielectric constant of the guide is.

Let us now consider the following questions.

Why is the attenuation constant for the TM-like mode so much smaller than that for the TE-like mode on the same thin ceramic ribbon guide?

The dip in the power distribution inside the ribbon guide for the TM-like mode means that most of the guided power is being carried in the lossless outside region while the mode is still firmly anchored to the ceramic slab. The guided modal power drops to less than 1 percent of the power strength at the ribbon boundary in less than  $0.5\lambda_0 = 0.38$  cm away from that boundary. As shown in Fig. 15(b), the guidance of the dominant TE-like mode along a ceramic ribbon follows the expected traditional manner discussed above. The presence of high power intensity within the thin dielectric slab implies that the attenuation constant of the TE-like mode is governed mostly by the loss tangent of the dielectric material and that the ribbon is not a low-loss geometry for a TE-like mode.

Why is a circular ceramic guide not a low-loss configuration?

It is known that the dominant mode on a circular ceramic guide is a hybrid mode [5–8], i.e., all six components of the electromagnetic fields are present. Calculation of the guided-power intensity

distribution for the dominant mode [17] shows the traditional pattern with the guided-power intensity peaking in the center of the guide and falling off radially as the distance from the guide increases. The pattern persists as the radius of the guide becomes smaller. This behavior implies, in the same way as the case of TE-like wave guidance along a thin ceramic ribbon, that the attenuation constant of the hybrid mode on a circular ceramic guide is governed mostly by the loss tangent of the dielectric material and that the circular ceramic guide is not a low-loss geometry for the hybrid mode.

Why is a lower dielectric-constant ribbon not a low-loss guidance structure?

To learn if the special power-intensity distribution that gives rise to the low-loss behavior of the dominant TM-like mode along a ceramic ribbon remains for low-dielectric-constant polymer ribbon, Fig. 15(c) is generated. In this figure, low-dielectric-constant Teflon slabs with  $\epsilon_1 = 2.04$  are used. Unlike the case for the TM-like mode propagation along a ceramic ribbon, a significant amount of power remains inside the Teflon ribbon. This is seen by the amount of red and orange colors that remains within the core of the Teflon ribbon. This means that a significant amount of attenuation for the TM-like mode is caused by the power carried within the core region of the Teflon ribbon. So, even for the TM mode, the Teflon ribbon is not a very good low-loss guidance structure as compared with the ceramic ribbon. Lowering the dielectric constant of the ribbon appears to have a significant negative effect on preserving the low-loss characteristics of a ribbon guide.

The guidance of the dominant TE-like mode along a ceramic ribbon follows the expected traditional manner wherein the guided-power intensity of the mode tends to peak in the middle of the guide and fall off as one moves away from the guide boundary. See Fig. 15(c). This behavior remains regardless of how thin the ribbon becomes or how large the dielectric constant of the guide is. The presence of high power intensity within the thin dielectric ribbon implies that the attenuation constant of the TE-like mode is governed mostly by the loss tangent of the dielectric material and that the ribbon is not a low-loss geometry for a TE-like mode. It appears that, for the TE-like mode, the general power-distribution characteristics stay the same for high-dielectric-constant ceramic ribbon or for low-dielectric-constant Teflon ribbon.

## VI. Conclusion

A new ultra-low-loss dielectric waveguide for millimeter/submillimeter waves has been found. It is a high-dielectric-constant ribbon with a dielectric constant of 10 and an aspect ratio of 10:1.

The measured data show that indeed the geometrical factor,  $\epsilon_1 R$ , of a dielectric waveguide plays a very important role in reducing the attenuation constant of a TM-like mode on a dielectric waveguide provided that the dielectric constant is *high* and the loss tangent is *low*. It also is shown that the dielectric ribbon is the preferred configuration for low-loss guidance. For example, for the same normalized cross-sectional area, say  $A(\epsilon_1 - 1)/\lambda_0^2 = 0.4$ , where  $A$  is the cross-sectional area of the dielectric waveguide and  $\lambda_0$  is the operating frequency, the attenuation constant of the dominant TM-like mode on a 10:1 aspect-ratio ribbon alumina waveguide is 140 times smaller than that on a circular alumina rod waveguide, even though the same amount of alumina material was used to construct these waveguides. The significance of the configuration factor is clear! With the data presented in this article, this fact has now been verified experimentally.

In conclusion, one notes that the way in which power is guided along a high dielectric constant ( $\epsilon_1 = 10$ ) and the thin ribbon-like structure are instrumental in providing an attenuation constant for the dominant mode of less than 10 dB/km in the 30- to 300-GHz spectrum range using Coors' 998 pure alumina material. The dominant TM-like mode is capable of "gliding" along the surface of the ribbon with exceedingly low attenuation and with a power pattern having a dip in the core of the ribbon guide. This feature makes the ceramic ribbon a true "surface" waveguide structure wherein the wave is guided

along adhering to a large surface with only a small amount of power being carried within the core region of the structure.

Just as the first 20-dB/km optical fiber made in the late 1960s produced a revolution in optical communication, so may the attainment of 10-dB/km ceramic ribbon provide an opening to the 30- to 300-GHz communication world.

## Acknowledgments

We wish to thank Charles Stelzried, Al Bhanji, Dan Rascoe, and Mark Gatti of JPL for their enthusiastic encouragement and support. Expert assistance from Richard Cirillo on experimental measurements and from Cynthia Copela in graphic works is greatly appreciated.

## References

- [1] K. C. Kao and G. A. Hockman, "Dielectric Fiber Surface Waveguides for Optical Frequencies," *Proc. IEE*, vol. 133, pp. 1151–1158, 1966.
- [2] M. N. Afsar and K. J. Button, "Millimeter-Wave Dielectric Measurement of Materials," *Proc. IEEE*, vol. 73, pp. 131–153, 1985.
- [3] R. Birch, J. D. Dromey, and J. Lisurf, "The Optical Constants of Some Common Low-Loss Polymers Between 4 and 40  $\text{cm}^{-1}$ ," *Infrared Physics*, vol. 21, pp. 225–228, 1981.
- [4] M. N. Afsar, "Precision Dielectric Measurements of Nonpolar Polymers in Millimeter Wavelength Range," *IEEE Trans. Microwave Theory and Tech.*, vol. MTT-33, pp. 1410–1415, 1985.
- [5] C. Yeh, "Dynamic Fields", in *American Institute of Physics Handbook*, 3rd ed., D. E. Gray, editor, New York: McGraw Hill, 1972.
- [6] S. Ramo, J. R. Whinnery, and T. Van Duzer, *Fields and Waves in Communication Electronics*, 2nd ed., New York: John Wiley Book Co., 1984.
- [7] C. Yeh, "Elliptical Dielectric Waveguides," *J. Appl. Phys.*, vol. 33, pp. 3235–3243, 1962.
- [8] C. Yeh, "Attenuation in a Dielectric Elliptical Cylinder," *IEEE Trans. Antenna and Propagation*, vol. AP-11, pp. 177–184, 1963.
- [9] C. Yeh, K. Ha, S. B. Dong, and W. P. Brown, "Single-Mode Optical Waveguides," *Applied Optics*, vol. 18, no. 10, pp. 1490–1504, 1979.
- [10] A. Taflove, *Computational Electrodynamics, the Finite-Difference Time-Domain Method*, Norwood, Massachusetts: Artech House, 1995.
- [11] C. Yeh, L. Casperson, and B. Szejn, "Propagation of Truncated Gaussian Beams in Multimode Fiber Guides," *Journal of the Optical Society of America*, vol. 68, no. 7, pp. 989–993, 1978.

- [12] C. Yeh, F. I. Shimabukuro, and J. Chu, "Ultra-Low-Loss Dielectric Ribbon Waveguide for Millimeter/Submillimeter Waves," *Appl. Phys. Lett.*, vol. 54, pp. 1183–1185, 1989.
- [13] S. K. Koul, *Millimeter Wave and Optical Dielectric Integrated Guides and Circuits*, Wiley Series in Microwave and Optical Engineering, New York: Wiley, 1997.
- [14] F. I. Shimabukuro and C. Yeh, "Attenuation Measurement of Very Low Loss Dielectric Waveguides by the Cavity Resonator Method Applicable in the Millimeter/Submillimeter Wavelength Range," *IEEE Trans. on Microwave Theory and Techniques*, vol. 36, pp. 1160–1166, 1988.
- [15] C. Yeh, "A Relation Between  $\alpha$  and  $Q$ ," *Proc. IRE*, vol. 50, p. 2145, 1962.
- [16] Coors Ceramics Company, Electronic Products Group, Golden, Colorado, 1999.
- [17] C. Yeh and G. Lindgren, "Computing the Propagation Characteristics of Radially Stratified Fibers: An Efficient Method," *Appl. Opt.*, vol. 16, pp. 483–493, 1977.